Ultrathin Perovskite Monocrystals Boost the Solar Cell Performance

Wenchi Kong, Shiwei Wang, Feng Li, Chen Zhao, Jun Xing, Yuting Zou, Zhi Yu, Chun-Ho Lin, Yuwei Shan, Yu Hang Lai, Qingfeng Dong, Tom Wu, Weili Yu,* and Chunlei Guo*

Grains and grain boundaries play key roles in determining halide perovskite-based optoelectronic device performance. Halide perovskite monocrystalline solids with large grains, smaller grain boundaries, and uniform surface morphology improve charge transfer and collection, suppress recombination loss, and thus are highly favorable for developing efficient solar cells. To date, strategies of synthesizing high-quality thin monocrystals (TMCs) for solar cell applications are still limited. Here, by combining the antisolvent vapor-assisted crystallization and space-confinement strategies, high-quality millimeter sized TMCs of methylammonium lead iodide (MAPbI$_3$) perovskites with controlled thickness from tens of nanometers to several micrometers have been fabricated. The solar cells based on these MAPbI$_3$ TMCs show power conversion efficiency (PCE) of 20.1% which is significantly improved compared to their polycrystalline counterparts (PCE) of 17.3%. The MAPbI$_3$ TMCs show large grain size, uniform surface morphology, high hole mobility (up to 142 cm^2 V^{-1} s^{-1}), as well as low trap (defect) densities. These properties suggest that TMCs can effectively suppress the radiative and nonradiative recombination loss, thus provide a promising way for maximizing the efficiency of perovskite solar cells.

Organic/inorganic hybrid perovskites have emerged as highly efficient solar cell materials and achieved a staggering 25.2% power conversion efficiency (PCE) in the past few years.[1–5] However, the record efficiency is still lower than the detailed balance model predicted by Shockley–Queisser which believe the efficiency limit of perovskite solar cells can go up to 31%.[6] It is necessary to overcome the bottleneck that hinders the performance of perovskite solar cells. Up to date, most of the reported solar cells are based on perovskite polycrystalline films (PCFs). In 2015, Ginger and coworkers found that the centre of perovskite grains produce a much stronger luminescence signal than photoexcitation in the vicinity of grain boundaries, which indicates that there is an accelerated trap-assisted charge recombination in the boundary areas.[7] This finding was further proved by the reports that claimed the grain size is critical for achieving high solar conversion efficiency and large grain size leads to high PCE.[8–12] These reports suggest that the performance of perovskite solar cells may be further improved by enlarging the grain size and decreasing the grain boundaries.[13] Considering that Si single-crystal cell has provided an instructive example that bulk crystal can maximize the PCE,[14] we believe that synthesizing perovskites with grain size to millimeters or above with controlled thickness and the surface morphology would be a promising strategy to maximize the performance of perovskite solar cells.

W. Kong, C. Zhao, J. Xing, Y. Zou, Dr. Z. Yu, Dr. Y. Shan, Dr. Y. H. Lai, Prof. W. Yu
The Guo Photonics Laboratory
State Key Laboratory of Applied Optics
Changchun Institute of Optics
Fine Mechanics and Physics
Chinese Academy of Sciences
Changchun 130033, China
E-mail: weili.yu@ciomp.ac.cn
W. Kong, C. Zhao, J. Xing, Y. Zou, Dr. Z. Yu, Dr. Y. Shan, Dr. Y. H. Lai, Prof. W. Yu
University of Chinese Academy of Sciences
Beijing 100049, China
Prof. S. Wang
School of Chemical Engineering
Changchun University of Technology
Changchun 130012, China

Prof. F. Li
School of Physics
the University of Sydney
Sydney, NSW 2006, Australia
Dr. C.-H. Lin, Prof. T. Wu
School of Materials Science and Engineering
University of New South Wales
Sydney, NSW 2052, Australia
Prof. Q. Dong
State Key Laboratory of Supramolecular Structure and Materials
College of Chemistry
Jilin University
Changchun 130012, China
Prof. C. Guo
The Institute of Optics
University of Rochester
Rochester, NY 14627, USA
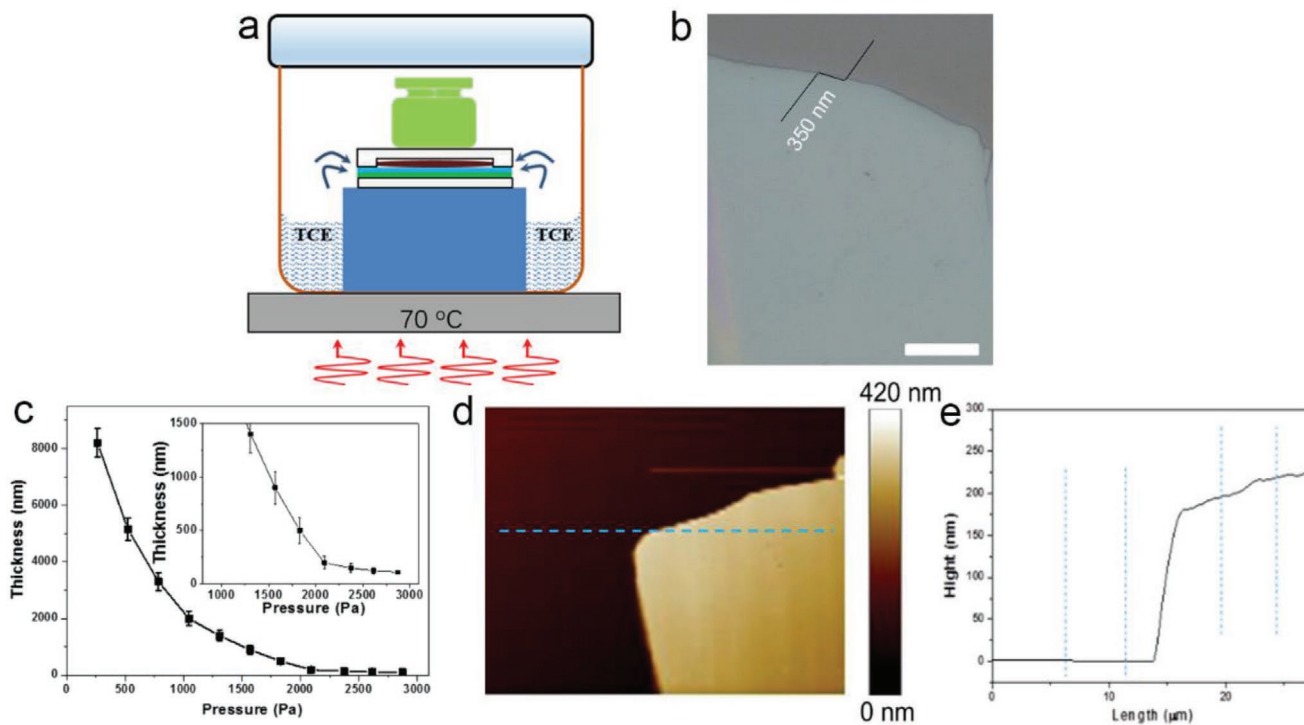E-mail: chunlei.guo@rochester.edu

Figure 1. a) The schematic diagram of TMC perovskite incubating process. b) One optical image of incubated perovskite TMC. Scale bar: 50 μm. c) The dependance of TMC thickness on applied pressure. d) The AFM image of TMC edge, which shows the sharp edge of MAPbI₃ TMC with a thickness of around 230 nm. e) The cross section profile of TMC along the blue line as shown in (d).

Halide perovskite bulk single crystals have been reported to have low trap densities ($\approx 10^{10}$ cm^{-3} for $CH_3NH_3PbI_3$ and $\approx 10^9$ cm^{-3} for $CH_3NH_3PbBr_3$).[15,16] Combining their excellent properties, such as large absorption coefficient, high charge carrier mobility, and large exciton diffusion length, the perovskite single crystals thus hold a great possibility to maximize solar cell device performance once suitable thickness can be achieved. Some research groups have conducted pioneering investigations in this direction. The Osman group developed a thin monocrystals (TMCs) growth method utilizing a cavitation-triggered asymmetrical crystallization strategy to fabricate $CH_3NH_3PbBr_3$ single crystals with 2 μm thickness.[17] The Liu group employed an ultrathin geometry-defined dynamic-flow reaction system and achieved 150 μm thick single crystals.[18] Furthermore, Hu and coworkers reported controllable fabrication of sub-millimeter-size, air-stable perovskite single crystal thin films with the thickness adjustable from nano- to micrometers with an aspect ratio up to $\approx 10^5$.[19] Chen et al. fabricated perovskite solar cells based on 10 μm single crystals and achieved improved efficiency after surface modification.[20,21] Very recently, Dong group demonstrated stable and efficient later-structure perovskite.[22] An illuminating statistical paper based on the single crystals from the Chen group called for more research activities in this emerging field.[23]

Here, we demonstrated methylammonium lead iodide ($CH_3NH_3PbI_3$) TMCs with tunable thickness from several hundred nanometers to several micrometers by combining the antisolvent vapor-assisted crystallization (AVC) and the space-confinement strategy. Efficient perovskite solar cells were then fabricated based on the synthesized TMCs. The PCE of our developed perovskite solar cells improved significantly from 17.3% based on PCF perovskites to 20.1% based on TMCs. The surface and cross-section morphology, carrier lifetime, and surface photoluminescence dynamic analysis highlighted the advantages of TMCs in minimizing light-emitting loss and potential for developing high-efficiency, solar cells as well as photodetectors, sensors, and phototransistors.

The solution-grown MAPbI₃ TMCs were prepared using AVC method at the temperature of 70 °C with trichloroethane (TCE) as antisolvent.[12] The scheme of synthesizing perovskite TMC is shown in **Figure 1**a. The PEDOT:PSS spin-coated ITO/glass worked as the substrate, and a silica cover with controlled loading weight was used to tune the thickness of perovskite TMCs. A thin layer of (3-aminopropyl) triethoxysilane (APTES) was self-assembled on the surface of the silica cover, which could produce a hydrophobic surface and avoid the TMC attaching on the silica cover. After 48 h, TMCs with the thickness of 350 nm were formed on ITO/PEDOT:PSS substrate (Figure 1b). The pentadeuterophenyl-C61-butyric-acid-methyl ester (PC₆₁BM) solution in chlorobenzene (15 mg mL^{-1}) and bathocuproine (BCP) in isopropanol (2 mg mL^{-1}) were then spin-coated on the top of TMC in sequence to form the electron transport layer. After drying in vacuum chamber overnight, 120 nm Ag was thermally deposited on the top as cathode for the solar cells. The thickness of TMC can be tuned by controlling the perovskite solution concentration and the loading weight on the silica cover.[19] The dependence of TMC thickness on loading weight is shown in Figure 1c, indicating that
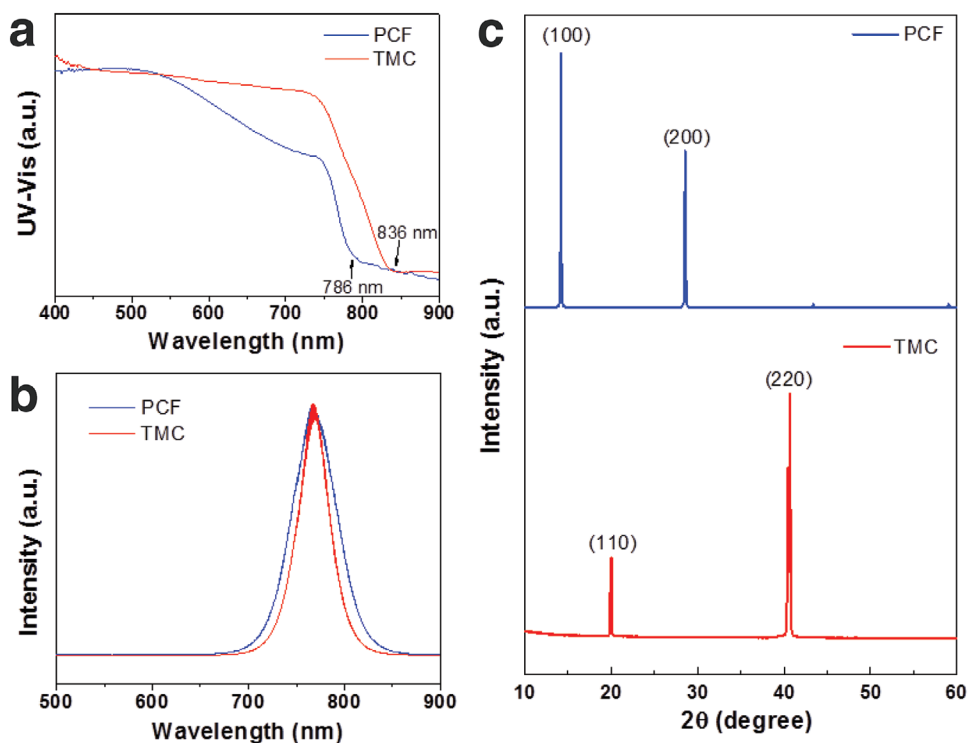
Figure 2. a) UV–vis, b) photoluminescence, and c) XRD spectra of PCF and TMC MAPbI$_3$ films, respectively.

the TMC thickness decreases continuously with the increasing of loading weight and finally gets stabilized. The atomic force microscope (AFM) image of one of the thinnest crystals and the related height profile are shown in Figure 1d,e, which indicates that the thickness is around 230 nm. The surface height curves of MAPbI$_3$ PCF and TMC are presented in Figure S1, Supporting Information. The photograph of TMC in different stages are displayed in Figure S2, Supporting Information, and the photograph of TMC with different thicknesses are shown in Figure S3, Supporting Information. More scanning electron microscope (SEM) images of perovskite TMC with different thicknesses are shown in Figure S4, Supporting Information, the corresponding thickness of AFM is shown in Figure S5, Supporting Information. The optical properties and structure of perovskite TMC were then characterized and compared with its PCF counterparts. The light absorbance spectra are shown in **Figure 2**a. The absorption of PCF film starts at 786 nm, while that of the TMC starts at 836 nm. The extended absorption range and the clear band edge cutoff of the perovskite TMC can be attributed to the long-range structural coherence.[24] The gradually increased absorbance of PCFs suggests the existence of in-gap defect states.[15] The photoluminescences (PLs) of both samples are presented in Figure 2b, from which both peaks were found to center at 768 nm. The full width at half maximum of PL for TMC is 40.2 nm, compared with that of 56.4 nm for PCF. As PL is closely connected with surface-charge recombination,[25,26] the narrow PL response of TMC sample indicates the less surface-charge recombination centers due to less grain boundaries and well-protected surfaces. X-ray diffraction (XRD) measurements demonstrate high purity of crystalline perovskite phase for both samples (Figure 2c). The

PCF shows strong peaks at 14.2° and 28.5°, which were indexed to (100) and (200) faces of cubic phase, while TMC presents two peaks at 20.2° and 40.6°, which matches well with (110) and (220) faces of CH$_3$NH$_3$PbI$_3$ perovskite, respectively.[27,28] Both samples XRD patterns match well with the cubic structure,[29] and the different peak positions between two samples may imply that the preferred orientation of perovskite varies under different forming processes, which may be attributed to the crystallization kinetics by accommodating the difference in the precursor-solvent interaction and temperatures.[30] The (110) peak of TMC displays a small full-width at half maximum of 0.28° from φ scan curve in Figure S6, Supporting Information, that confirms the good quality of TMC.[20,31]

We then characterized the morphologies of both TMC and PCF MAPbI$_3$ films. As shown in **Figure 3**a, the SEM of PCF top surface showed plenty of grains with the average size around 250 nm. Figure 3b shows the top surface SEM image of TMC, and there are no grains and grain boundaries, which will greatly decrease the possibility of charge trapping or recombination. The cross-section morphologies of both perovskite samples are shown in Figure 3c,d. The SEM image indicates that the TMC layer is monocrystal structured with thickness around 300 nm and no grain boundaries. While the PCF is polycrystalline and shows some grains. As the grain boundaries were reported to serve as nonradiative recombination centers in polycrystalline semiconductor films,[7] the monocrystal perovskites without grain boundary are thus highly preferred for avoiding carrier recombination loss.

The surface morphology of perovskite was further characterized by AFM measurements. The surface morphology of PCFs is composed of tiny grains with an average size of around 250 nm
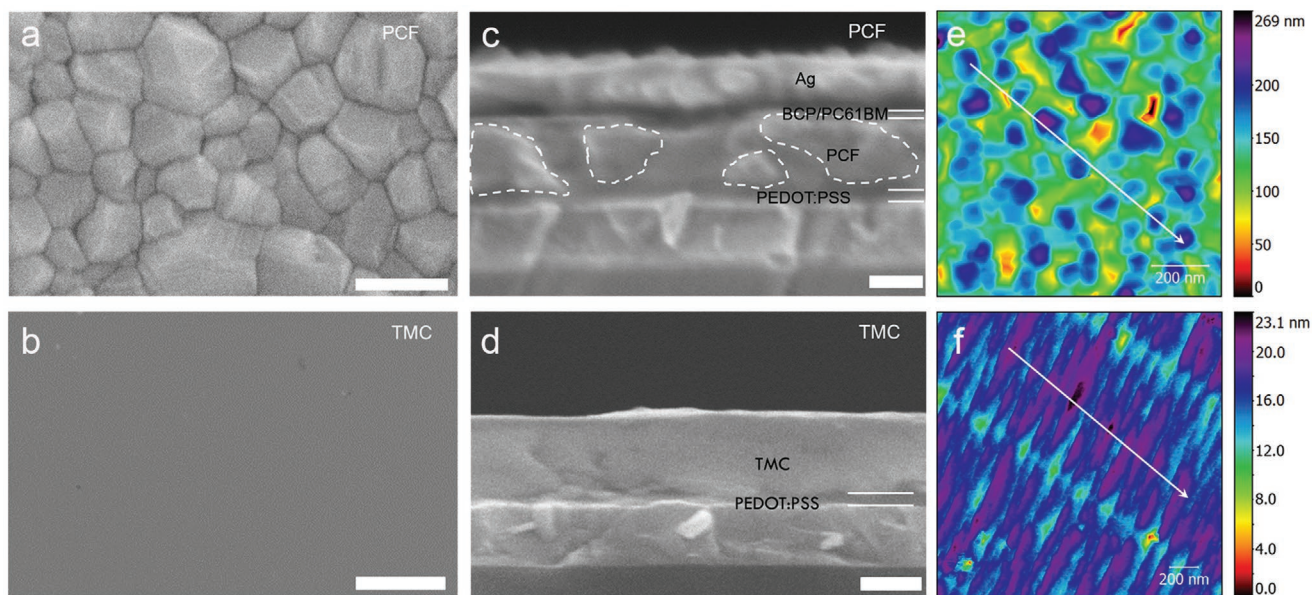
Figure 3. SEM images of top surface of a) PCF and b) TMC perovskites. Scale bar: 300 nm. And cross-section SEM images of MAPbI$_3$ samples based on c) PCF and d) TMC, respectively. Scale bar: 250 nm. AFM images of the MAPbI$_3$ e) PCF and f) TMC surfaces, respectively. The straight lines in (e) and (f) show the surface profiles of PCF and TMC samples, respectively, and are presented in Figure S1, Supporting Information.

(Figure 3e), which is corresponding well to the SEM image as shown in Figure 3a. The TMCs surface shows some ripple dunes with the length of over 1 μm and width of over 100 nm and no grain boundaries (Figure 3f). The unique surface morphology of TMCs can be attributed to solvent vapor transportation during the crystal growing process. More importantly, the root mean square roughness of PCF is 32.8 nm, which is much

larger than that of TMC (2.1 nm). The smooth surface implies that the TMC films have more chances to prevent leakage happening, thus being favorable for the charge collection.

Perovskite solar cells based on both MAPbI$_3$ PCF and TMC were fabricated. The structure of perovskite solar cells is shown in **Figure 4**a, and the energy band alignment is presented in Figure 4b. The PC$_{61}$BM (40 nm) and the BCP (6 nm) layers
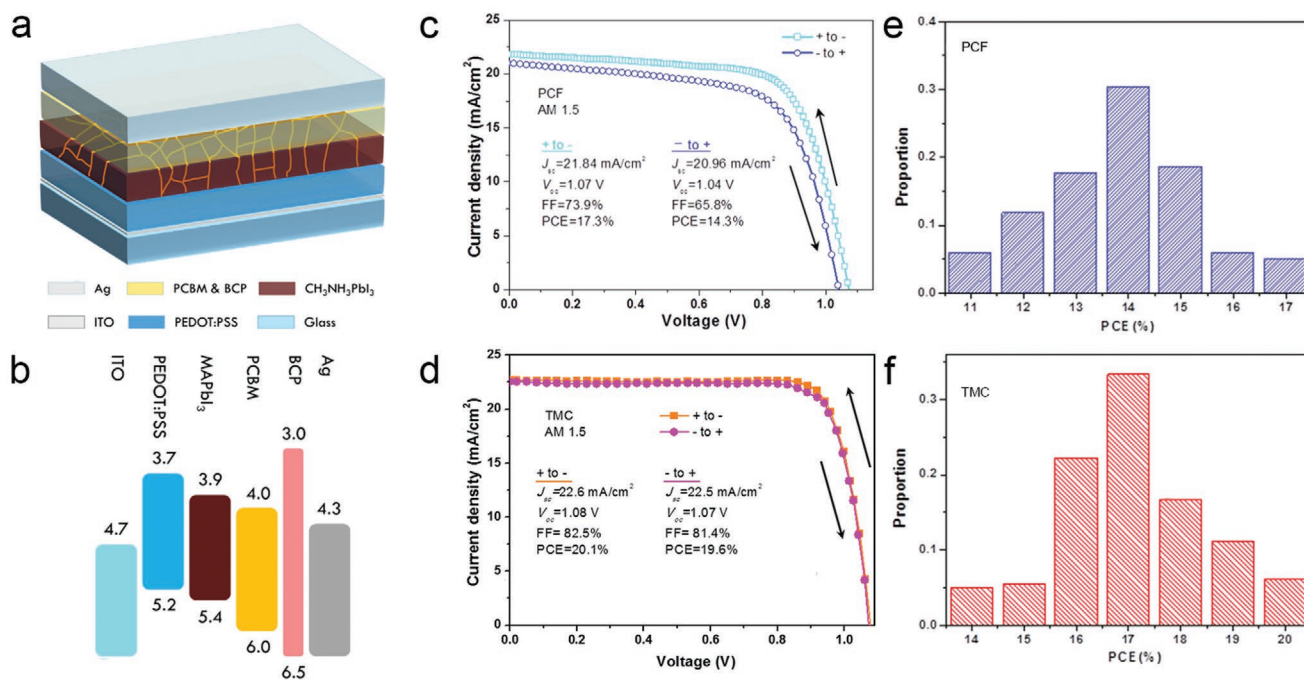

Figure 4. a) The device structure of the perovskite solar cells. b) The energy alignments of the device. Unit of values: eV. c,d) The current density versus voltage performance of MAPbI$_3$ solar cells based on PCF and TMC, respectively. The PCE distribution was shown in (e) and (f).

**ADVANCED
SCIENCE NEWS**

www.advancedsciencenews.com

**ADVANCED
ENERGY
MATERIALS**

www.advenergymat.de

were utilized as electron transport layer. In Figure 4c, we present the J–V curves of solar cells based on MAPbI$_3$ PCF, which shows a PCE of 17.3% as the applied voltage scans from positive to negative. The J–V curves of solar cells based on the perovskite TMC are shown in Figure 4d, and the PCE goes up to 20.1% under the same experimental setup. The open circuit voltage (V_{oc}), short circuit current (J_{sc}), fill factor (FF), and PCE of TMC-based solar cells are all improved compared to those of PCF-based devices. In details, V_{oc} improves from 1.07 to 1.08 V, J_{sc} increases greatly from 21.8 to 22.6 mA cm^{-2}, and the FF enhances from 73.9% (for PCF) to 82.5% (for TMC). The high FF is believed to be resulting from the smooth surface of perovskite layer.[32] The shunt resistances of PCF and TMC sample are 570 and 4250 Ω, that is consistent with FF from 73.9% to 82.5%. The serial resistances of PCF and TMC sample are 14.5 and 5.6 Ω, these matches with PCE. External quantum efficiency (EQE) of solar cells based on both TMC and PCF are provided in Figure S7, Supporting Information. The statistical distribution of PCE for both PCF and TMC based solar cells are shown in Figure 4e,f, where the TMC devices show an average PCE of 17.2% compared with the PCF devices (14%). The stability of both PCF and TMC solar cells are presented in Figure S8, Supporting Information. For TMC solar cells, the J_{sc} and PCE decrease less than 7% after 30 days, while those of the PCF solar cells decrease 14.3%, indicating that the TMC devices have better resistance to humidity in the air. The degradation property of perovskite solar cells can be attributed to the surface morphology. The much rougher surface with small grain size and more grain boundaries of PCF perovskite makes the erosion happen more easily.[33,34] Hysteretic phenomena have been commonly observed in the halide perovskite solar cells, and it has been speculated to originate from trapping/de-trapping of charge carriers,[35] ferroelectricity,[36,37] changes in absorber/contact conductivity,[38] and ion migration.[39] In these cases, the crystal defects and ion migration are believed to be the main causes of the hysteresis effect. As shown in Figure 4c,d, the hysteresis was found to exist in both PCF and TMC devices, and the hysteresis effect in latter device is much weaker than that in the former one. When the voltage scanning direction is switched, the photocurrent change in PCF solar cells is larger than that in TMC, especially when voltage is above 0.5 V. The PCE change is calculated to be 3% for PCF, while the TMC reveals a PCE variation of 0.5%. It is a consensus that the perovskite layer has both free electrons and ion carriers, and the polarization of ions plays a key role here. The reduction of carrier trapping induced polarization at the grain boundary is believed to be the main reason for the hysteresis relieve in the TMC films.[38,40]

The schemes of carrier transfer and recombination are shown in **Figure 5**a,b. For PCF, when a bias is applied on the film in the vertical direction, the tunnels between the grains would accumulate free charges or ions at the grain boundaries, resulting in the change of electric field distribution.[41] And the existing grains and grain boundaries would trap more carriers and lead to more recombinations, causing a significant PCE loss. For TMC, there are no grains and grain boundaries, thus weakening the hysteresis effect in the vertical direction. As the ions have much smaller mobility ($1.5 \times 10^{-9} \pm 0.5 \times 10^{-9}$ cm^2 V^{-1} s^{-1}) compared to the free charges (0.18 cm^2 V^{-1} s^{-1} for holes and

0.17 cm^2 V^{-1} s^{-1} electrons),[42,43] once the direction of bias is switched, the polarized charges and ions will drift in different speeds, leading to the hysteresis phenomenon. For the high-quality TMC, there are no grains and grain boundaries so that the carriers can pass through the crystals more efficiently. To compare the integrated fluorescence intensity, we performed PL mapping to examine the difference between TMC and PCF samples. The samples were illuminated with 532 nm laser, and the PL mapping for both TMC and PCF perovskite films are shown in Figure 5c,d, respectively. The scheme of electronic energy levels and three optional procedures carrier may endure in perovskites are shown in Figure 5e. First, charge carriers can be quenched at grain boundaries or defects under non-radiative recombination. Second, the charge carriers (including electrons in conduction band and holes in valence band) can produce fluorescence through radiative recombination. Third, the charge carriers separate into free electrons and holes, and form directional movement.[44] For PCF, smaller grains can spatially limit the diffusion length of charge carriers or free electrons and holes, which makes it easier for the electrons to combine with the holes, that leads to an increase of radiative recombination inside the grains, producing high PL intensity. On the contrary, for TMC, the large grain makes charge carriers have a long diffusion length and more charge carriers separate into free electrons and holes, and form directional movement, instead of radiative recombination,[45] so PL intensity of PCF sample is much higher than that of TMC. More charge carriers separate into free electrons and holes which is favorable process for the high-efficiency perovskite solar cell. This is consistent with the improvement of PCE for TMC comparing with PCF.

To explore the carrier recombination dynamics in the MAPbI$_3$ layer, time-resolved photoluminescence (TRPL) measurements were conducted. TRPL can be fitted with tri-exponential decay function and the carrier lifetime can be obtained from three decay processes (including fast, middle, and slow process).[46] The carrier lifetimes (τ_1, τ_2, τ_3), fractional contributions (f_1, f_2, f_3), and calculated average carrier lifetime ($\tau_{ave} = \tau_1 f_1 + \tau_2 f_2 + \tau_3 f_3$),[47] τ_{ave} of PCF and TMC range from 19.42 to 67.47 ns, are shown in Figure 5f. The short lifetime (τ_1) represents surface lifetime, the middle lifetime (τ_2) represents transition lifetime, and the long lifetime (τ_3) represents bulk lifetime.[48] For PCF and TMC, τ_1, τ_2, τ_3 increases from 5, 23, and 63 ns to 8, 44, and 132 ns. Importantly, the fractional contributions f_1 for τ_1 in TMC is significantly lower than that of PCF, the fractional contributions f_3 for τ_3 in TMC is significantly higher than that of PCF, This further confirms that the defect density of the TMC is significantly lower than that of the PCF both in the surface layer and the bulk layer, the finally calculated average carrier lifetime also illustrates this conclusion. As highly efficient exciton separation and charge collection are preferred in solar cells, the large lifetime of τ_{ave} in TMC indicates that the photo-generated charges have more opportunities to be efficiently transferred in TMC and to be collected at the TMC/electrode interfaces, which matches well with the improved efficiency of TMC solar cells.[49,50] Note that previous research have reported that perovskite single crystals have much longer carrier lifetime,[15,16] we believe that this may be attributed to the ultrathin monocrystals and the existing of interface layers between perovskites and electrodes.
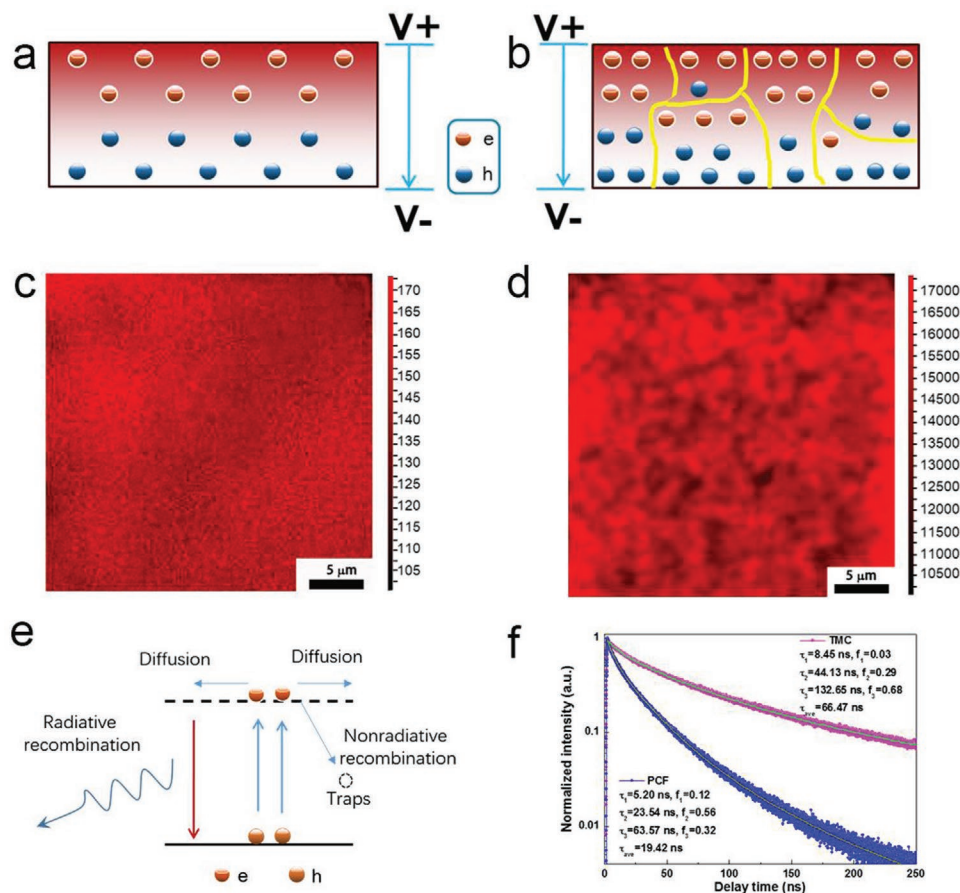
Figure 5. The schemes of carrier transfer in a) TMC and b) PCF films under vertically applied voltages. PL mapping figures of c) TMC and d) PCF perovskite films. The figures indicate that the PL intensity distribution of the PCF surface is two orders of magnitude higher than that of the TMC films. The samples were illuminated with 532 nm laser and PL intensity was recorded with Horiba Raman spectrometer. e) The scheme of molecular electronic state energy levels and carrier transfer paths in perovskites. f) The TRPL spectra of TMC and PCF samples.

We also performed space charge limited current (SCLC) experiments to reveal the trap density of the perovskite layers. With the structure of ITO/PEDOT:PSS/MAPbI$_3$/Au, we measured the $I-V$ responses for both PCF and TMC samples, from which the hole mobilities and trap densities can be calculated. As shown in Figure S9, Supporting Information, the $I-V$ curve of the TMC sample shows clear three regions. The hole mobility of 142 cm^2 V^{-1} s^{-1} and the trap density of 2.23×10^{11} cm^{-3} are extracted from child region and trap-filled limit region, respectively. The hole mobility is much higher than the early reports by Shi and Dong reports.[15,16] Although the trap density is a little bit larger than bulk single crystals, it's two orders of magnitude less than the polycrystalline Si ($N_{traps} \approx 10^{13}$ to 10^{14} cm^{-3}),[15,51] indicating the high purity of TMC layer. For the PCF sample, however, no quadratic relationship between current and applied voltage could be achieved most probably due to the large amounts of grains, which interdicts the carrier transfer. These results suggest that the TMC samples have less trap (defect) states and can effectively eliminate the nonradiative recombination loss. From the transient photocurrent (TPC), the charge-transport time obtained to be 463 ns shows faster charge transport.[52] Due to the reduced trap density

resulted in larger carrier mobility, which further resulted in quicker charge extraction for TMC sample in the Figure S10a, Supporting Information.[52–54] In the meanwhile, from the transient photovoltage (TPV) in the Figure S10b, Supporting Information, the charge recombination lifetime obtained to be 58 µs shows slower interfacial charge recombination,[20,53] which explains that faster carrier extraction prevents charge accumulation at the perovskite-charge extraction layer interface.[20,52,53] This result is consistent with SCLC. In summary, we demonstrated MAPbI$_3$ monocrystals with tunable thickness via two substrates confined AVC method. The solar cells based on 300 nm thick MAPbI$_3$ monocrystals showed improved solar energy conversion efficiency compared to their polycrystalline counterparts. The improved performance is attributed to the large grain size which effectively suppressed the grain boundaries induced radiative and nonradiative recombination loss, thus significantly improves the charge transfer property and carrier collection efficiency. This TMC fabrication technique can be generalized to other perovskite materials, promising to boost the performance of not only solar cells, but also photodetectors, phototransistors, and light-emitting diodes, as single crystal silicon did.

Experimental Section

Chemicals: The CH_3NH_3I was purchased from Dyesol and used as received. TCE, dimethylformamide, APTES, pentadeuterophenyl-C61-butyric-acid-methyl ester ($PC_{61}BM$) and γ-butyrolactone (GBL) were purchased from Sigma-Aldrich and used as received. Lead iodide (PbI_2) was acquired from Sigma-Aldrich and recrystallized twice before use. BCP was purchased from Jilin OLED company and used as received.

Thin Mono-Crystal Synthesis: The synthesis was conducted in air ambient. The $CH_3NH_3PbI_3$ TMC was grown via AVC protocol. Briefly, 5 µL $CH_3NH_3I_3$ (1 M) in GBL at 60 °C stirring overnight was dropped on ITO glasses covered with PEDOT:PSS layer (50 nm), which was followed by covering with silica substrate (2 × 2 cm^2, 2 mm thick) etched fixed thickness as a cover. The silica was first cleaned by rinsing with by acetone, isopropanol, and deionized water in turn. After drying in oven at 70 °C overnight, followed by an ultraviolet-ozone (UVO) surface treatment for 15 min, and then the recessed area in the silica was self-assembled with a thin layer of APTES by dipping the silica in APTES hexane solution (v/v = 1/500) for 1 min. The soaked silica was then quickly washed with acetone and blow-dried with nitrogen. The mix of detergent alconox and calcium acetate hydrate was used to wipe the edge of the silica. Similarly, PEDOT: PSS/ITO also wiped off the edge of the same area. Then the silica was covered on the PEDOT: PSS/ITO and placed in a vacuum drying oven at 60 °C, until the glass and silica were in close contact.[55] The solution will spread automatically between the substrates via surface tension force. The sealed beaker and the surface dish lid were cleaned by acetone, isopropanol, and deionized water in turn and drying in oven at 70 °C overnight. Then the surface dish lid cover was put inside the sealed beaker upside down, and the TCE was injected along the wall of the sealed beaker by using the pipette. Do not exceed the surface dish lid cover. Another surface dish lid bottom was put with the sample on the surface dish lid cover surrounded by TCE on the bottom, then steel beads of different weights placed in a vial were placed on the sample according to the thickness of the required film. Next, sealed beaker was covered with plastic wrap and sealed with sealing film, and heated under 70 °C till single crystal was formed in the hotplate. The solution of same volume was added for two or three more times to enlarge the size of crystals.

Device Fabrication: The ITO glasses were first cleaned by rinsing with acetone, isopropanol, and deionized water in turn. After drying in oven at 70 °C overnight, followed by an UVO surface treatment for 15 min, a PEDOT:PSS layer was spin-coated as previously reported.[56] The substrate was then used to grow $CH_3NH_3PbI_3$ TMC in ambient condition as described above. Then, in a nitrogen-filled glove box, after spin-coating PCBM (15 mg mL^{-1} in chlorobenzene) at 2500 rpm for 20 s, 6 nm BCP (2 mg mL^{-1} in isopropanol) was also spin coated at 5000 rpm for 30 s on top as electron transporting layer. Finally, 120 nm Ag was thermal evaporated as electrode in vacuum (<10^{-4} Pa). The size of active area was calculated to be 3 mm^2.

Characterization: UV–vis spectra were measured using a Cary 5000 spectrophotometer. The PL mapping spectra was recorded through a Horiba Raman spectrometry with 532 nm laser in air at room temperature. XRD was performed at room temperature using an X-ray diffractometer (D8 Discover, Bruker). AFM characterization was conducted on a Bruker's Dimension Icon system. SEM image was conducted on Hitachi S-4800 SEM and 2D SEM was taken on a Phenom ProX system. *I–V* curves were measured using keithley 2400 with the solar simulator from Sanyou Company. EQE was measured on a home-built system. The xenon lamp light source (HM-Xe500W) and the monochromator (HM-ISW151) were combined to form a monochromatic wavelength, and a power meter and keithley 2400 from Sanyou Company were used to monitor the energy and current by the monochromatic wave irradiated on the solar cell. SCLC measurements were conducted using keithley 2400 on the vertical samples, in which an 80 nm Au electrode was thermal evaporated onto the TMC on the ITO/glass substrate with masks. MicroTime 200 time-resolved fluorescence microscope (PicoQuant) was used to obtain TRPL spectra with 532 nm laser excitation at room temperature in air. For TPC and

TPV measurements, 355 nm laser pulse with 3–7 ns in width and low intensity was utilized, the repeating frequency was 10 Hz. The device was serially connected to a digital oscilloscope (MDO4104C) and the input impedance of the oscilloscope was set to 50 Ω and 1 MΩ, respectively, to form the short- and open-circuit conditions, respectively, for observing the charge extraction time and charge density decay. The TPC measurements was in the dark, the TPV was measured under 0.3 sun illumination.

Supporting Information

Supporting Information is available from the Wiley Online Library or from the author.

Conflict of Interest

The authors declare no conflict of interest.

[1] W. S. Yang, J. H. Noh, N. J. Jeon, Y. C. Kim, S. Ryu, J. Seo, S. I. Seok, *Science* **2015**, *348*, 1234.

[2] M. Saliba, T. Matsui, K. Domanski, J. Y. Seo, A. Ummadisingu, S. M. Zakeeruddin, J. P. Correa-Baena, W. R. Tress, A. Abate, A. Hagfeldt, M. Gratzel, *Science* **2016**, *354*, 206.

[3] K. A. Bush, A. F. Palmstrom, Z. S. J. Yu, M. Boccard, R. Cheacharoen, J. P. Mailoa, D. P. McMeekin, R. L. Z. Hoye, C. D. Bailie, T. Leijtens, I. M. Peters, M. C. Minichetti, N. Rolston, R. Prasanna, S. Sofia, D. Harwood, W. Ma, F. Moghadam, H. J. Snaith, T. Buonassisi, Z. C. Holman, S. F. Bent, M. D. McGehee, *Nat. Energy* **2017**, *2*, 17009.

[4] Q. Jiang, Y. Zhao, X. W. Zhang, X. L. Yang, Y. Chen, Z. M. Chu, Q. F. Ye, X. X. Li, Z. G. Yin, J. B. You, *Nat. Photonics* **2019**, *13*, 460.

[5] A. Y. Alsalloum, B. Turedi, X. P. Zheng, S. Mitra, A. A. Zhumekenov, K. J. Lee, P. Maity, I. Gereige, A. Alsaggaf, I. S. Rogan, O. F. Mohammed, O. M. Bakr, *ACS Energy Lett.* **2020**, *5*, 657.

[6] W. Shockley, H. J. Queisser, *J. Appl. Phys.* **1961**, *32*, 510.

[7] D. W. deQuilettes, S. M. Vorpahl, S. D. Stranks, H. Nagaoka, G. E. Eperon, M. E. Ziffer, H. J. Snaith, D. S. Ginger, *Science* **2015**, *348*, 683.

[8] J. H. Im, I. H. Jang, N. Pellet, M. Gratzel, N. G. Park, *Nat. Nanotechnol.* **2014**, *9*, 927.

[9] W. Y. Nie, H. H. Tsai, R. Asadpour, J. C. Blancon, A. J. Neukirch, G. Gupta, J. J. Crochet, M. Chhowalla, S. Tretiak, M. A. Alam, H. L. Wang, A. D. Mohite, *Science* **2015**, *347*, 522.

ADVANCED
SCIENCE NEWS

www.advancedsciencenews.com

ADVANCED
ENERGY
MATERIALS

www.advenergymat.de

[10] M. A. Haque, J. Troughton, D. Baran, *Adv. Energy Mater.* **2019**, *10*, 1902762.

[11] A. F. Castro-Mendez, J. Hidalgo, J. P. Correa-Baena, *Adv. Energy Mater.* **2019**, *9*, 1901489.

[12] M. U. Rothmann, W. Li, J. Etheridge, Y. B. Cheng, *Adv. Energy Mater.* **2017**, *7*, 1700912.

[13] U. Bach, *Nat. Chem.* **2015**, *7*, 616.

[14] M. A. Green, Y. Hishikawa, E. D. Dunlop, D. H. Levi, J. Hohl-Ebinger, M. Yoshita, A. W. Y. Ho-Baillie, *Prog. Photovoltaics* **2019**, *27*, 3.

[15] D. Shi, V. Adinolfi, R. Comin, M. J. Yuan, E. Alarousu, A. Buin, Y. Chen, S. Hoogland, A. Rothenberger, K. Katsiev, Y. Losovyj, X. Zhang, P. A. Dowben, O. F. Mohammed, E. H. Sargent, O. M. Bakr, *Science* **2015**, *347*, 519.

[16] Q. F. Dong, Y. J. Fang, Y. C. Shao, P. Mulligan, J. Qiu, L. Cao, J. S. Huang, *Science* **2015**, *347*, 967.

[17] W. Peng, L. F. Wang, B. Murali, K. T. Ho, A. Bera, N. Cho, C. F. Kang, V. M. Burlakov, J. Pan, L. Sinatra, C. Ma, W. Xu, D. Shi, E. Alarousu, A. Goriely, H. He, O. F. Mohammed, T. Wu, O. M. Bakr, *Adv. Mater.* **2016**, *28*, 3383.

[18] Y. C. Liu, Y. X. Zhang, Z. Yang, D. Yang, X. D. Ren, L. Q. Pang, S. Z. Liu, *Adv. Mater.* **2016**, *28*, 9204.

[19] Y. X. Chen, Q. Q. Ge, Y. Shi, J. Liu, D. J. Xue, J. Y. Ma, J. Ding, H. J. Yang, J. S. Hu, L. J. Wan, *J. Am. Chem. Soc.* **2016**, *138*, 16196.

[20] Z. L. Chen, Q. F. Dong, Y. Liu, C. X. Bao, Y. J. Fang, Y. Lin, S. Tang, Q. Wang, X. Xiao, Y. Bai, Y. H. Deng, J. S. Huang, *Nat. Commun.* **2017**, *8*, 1890.

[21] Z. L. Chen, B. Turedi, A. Y. Alsalloum, C. Yang, X. P. Zheng, I. Gereige, A. AlSaggaf, O. F. Mohammed, O. M. Bakr, *ACS Energy Lett.* **2019**, *4*, 1258.

[22] Y. Song, W. Bi, A. Wang, X. Liu, Y. Kang, Q. Dong, *Nat. Commun.* **2020**, *11*, 274.

[23] X. Cheng, S. Yang, B. Q. Cao, X. T. Tao, Z. L. Chen, *Adv. Funct. Mater.* **2020**, *30*, 1905021.

[24] J. J. Choi, X. H. Yang, Z. M. Norman, S. J. L. Billinge, J. S. Owen, *Nano Lett.* **2014**, *14*, 127.

[25] Y. J. Fang, Q. F. Dong, Y. C. Shao, Y. B. Yuan, J. S. Huang, *Nat. Photonics* **2015**, *9*, 679.

[26] H. H. Fang, S. Adjokatse, H. T. Wei, J. Yang, G. R. Blake, J. S. Huang, J. Even, M. A. Loi, *Sci. Adv.* **2016**, *2*, e1600534.

[27] T. J. Jacobsson, L. J. Schwan, M. Ottosson, A. Hagfeldt, T. Edvinsson, *Inorg. Chem.* **2015**, *54*, 10678.

[28] H. M. Zhu, Y. P. Fu, F. Meng, X. X. Wu, Z. Z. Gong, Q. Ding, M. V. Gustafsson, M. T. Trinh, S. Jin, X. Y. Zhu, *Nat. Mater.* **2015**, *14*, 636.

[29] T. Baikie, Y. N. Fang, J. M. Kadro, M. Schreyer, F. X. Wei, S. G. Mhaisalkar, M. Graetzel, T. J. White, *J. Mater. Chem. A* **2013**, *1*, 5628.

[30] L. Q. Xie, L. Chen, Z. A. Nan, H. X. Lin, T. Wang, D. P. Zhan, J. W. Yan, B. W. Mao, Z. Q. Tian, *J. Am. Chem. Soc.* **2017**, *139*, 3320.

[31] J. J. Zhao, G. L. Kong, S. L. Chen, Q. Li, B. Y. Huang, Z. H. Liu, X. Y. San, Y. J. Wang, C. Wang, Y. Zhen, H. D. Wen, P. Gao, J. Y. Li, *Sci. Bull.* **2017**, *62*, 1173.

[32] Q. Wang, Q. F. Dong, T. Li, A. Gruverman, J. S. Huang, *Adv. Mater.* **2016**, *28*, 6734.

[33] C. Quarti, E. Mosconi, J. M. Ball, V. D'Innocenzo, C. Tao, S. Pathak, H. J. Snaith, A. Petrozza, F. De Angelis, *Energy Environ. Sci.* **2016**, *9*, 155.

[34] H. Zhang, X. F. Qiao, Y. Shen, T. Moehl, S. M. Zakeeruddin, M. Gratzel, M. K. Wang, *J. Mater. Chem. A* **2015**, *3*, 11762.

[35] H. J. Snaith, A. Abate, J. M. Ball, G. E. Eperon, T. Leijtens, N. K. Noel, S. D. Stranks, J. T. W. Wang, K. Wojciechowski, W. Zhang, *J. Phys. Chem. Lett.* **2014**, *5*, 1511.

[36] T. M. Koh, K. W. Fu, Y. N. Fang, S. Chen, T. C. Sum, N. Mathews, S. G. Mhaisalkar, P. P. Boix, T. Baikie, *J. Phys. Chem. C* **2014**, *118*, 16458.

[37] S. Aharon, B. El Cohen, L. Etgar, *J. Phys. Chem. C* **2014**, *118*, 17160.

[38] E. L. Unger, E. T. Hoke, C. D. Bailie, W. H. Nguyen, A. R. Bowring, T. Heumuller, M. G. Christoforo, M. D. McGehee, *Energy Environ. Sci.* **2014**, *7*, 3690.

[39] J. M. Azpiroz, E. Mosconi, J. Bisquert, F. De Angelis, *Energy Environ. Sci.* **2015**, *8*, 2118.

[40] C. C. Stoumpos, C. D. Malliakas, M. G. Kanatzidis, *Inorg. Chem.* **2013**, *52*, 9019.

[41] Y. B. Yuan, T. Li, Q. Wang, J. Xing, A. Gruverman, J. S. Huang, *Sci. Adv.* **2017**, *3*, e1602164.

[42] Y. B. Yuan, J. Chae, Y. C. Shao, Q. Wang, Z. G. Xiao, A. Centrone, J. S. Huang, *Adv. Energy Mater.* **2015**, *5*, 1500615.

[43] F. Li, C. Ma, H. Wang, W. J. Hu, W. L. Yu, A. D. Sheikh, T. Wu, *Nat. Commun.* **2015**, *6*, 8238.

[44] Q. S. Dong, Y. T. Shi, K. Wang, Y. Li, S. F. Wang, H. Zhang, Y. J. Xing, Y. Du, X. G. Bai, T. L. Ma, *J. Phys. Chem. C* **2015**, *119*, 10212.

[45] H. C. Cho, S. H. Jeong, M. H. Park, Y. H. Kim, C. Wolf, C. L. Lee, J. H. Heo, A. Sadhanala, N. Myoung, S. Yoo, S. H. Im, R. H. Friend, T. W. Lee, *Science* **2015**, *350*, 1222.

[46] A. H. Slavney, T. Hu, A. M. Lindenberg, H. I. Karunadasa, *J. Am. Chem. Soc.* **2016**, *138*, 2138.

[47] J. R. Lakowicz, *Principle of Fluorescence Spectroscopy*, Springer, New York, USA **2006**.

[48] Y. T. Liu, H. Z. Lu, J. X. Niu, H. T. Zhang, S. T. Lou, C. L. Gao, Y. Q. Zhan, X. L. Zhang, Q. Y. Jin, L. R. Zheng, *AIP Adv.* **2018**, *8*, 095108.

[49] H. H. Fang, F. Wang, S. Adjokatse, N. Zhao, J. Even, M. A. Loi, *Light: Sci. Appl.* **2016**, *5*, e16056.

[50] X. Li, Z. Liang, H. Wang, S. Qiao, Z. Liu, H. Jiang, W. Chen, R. Yang, *J. Mater. Chem. A* **2019**, *8*, 1360.

[51] J. R. Ayres, *J. Appl. Phys.* **1993**, *74*, 1787.

[52] T. M. Jiang, Z. Chen, X. Chen, X. Y. Chen, X. H. Xu, T. Y. Liu, L. Z. Bai, D. X. Yang, D. W. Di, W. E. I. Sha, H. M. Zhu, Y. M. Yang, *ACS Energy Lett.* **2019**, *4*, 1784.

[53] Z. G. Xiao, Q. F. Dong, C. Bi, Y. C. Shao, Y. B. Yuan, J. S. Huang, *Adv. Mater.* **2014**, *26*, 6503.

[54] Y. H. Shao, Z. G. Xiao, C. Bi, Y. B. Yuan, J. S. Huang, *Nat. Commun.* **2014**, *5*, 5784.

[55] P. B. Allen, D. T. Chiu, *Anal. Chem.* **2008**, *80*, 7153.

[56] D. Y. Liu, T. L. Kelly, *Nat. Photonics* **2014**, *8*, 133.